ACTUATOR SURFACE MODEL AND BLADE RESOLVED SIMULATIONS OF AN ATTACK RECONNAISSANCE CLASS ROTOR IN HOVER AND FORWARD FLIGHT

Alexander Coyle, The University of Sydney, Sydney, Australia
Ben Thornber, The University of Sydney, Sydney, Australia

Abstract

Two novel simulation methodologies were used to compute the forces acting upon the rotor of an Attack Reconnaissance Class (ARC) helicopter in both hover and forward flight. The first of these is the Actuator Surface Model (ASM), a hybrid Computational Fluid Dynamics (CFD) technique that allows for complex simulations of rotors at a markedly lower computational cost than traditional blade-resolved methods without a significant reduction in accuracy. Blade resolved calculations were performed using The University of Sydney code Flamenco, which employs a combination of very high order accurate schemes with a novel Radial Basis Function (RBF) mesh motion method. This enabled high mesh quality to be maintained after changing the pitch of the blade. The ASM and Flamenco were validated against each other, as well as published experimental and simulation datasets. In hover, excellent agreement is found between all solvers. The ASM was also used to perform forward flight calculations, producing results accurate to the validation dataset.

1. NOTATION

Symbols

c	Rotor chord, m
C_Q	Integrated torque coefficient
C_q	Sectional torque coefficient
C_T	Integrated thrust coefficient
C_t	Sectional thrust coefficient
R	Rotor radius, m
r	Local radial position, m
y^+	Dimensionless wall distance
θ_0	Collective angle, deg
μ	Advance ratio

Acronyms:

ARC	Attack Reconnaissance Class
ASM	Actuator Surface Model
CFD	Computational Fluid Dynamics
RBF	Radial Basis Function

2. INTRODUCTION

The simulation of helicopter rotors using CFD is a complex task and often requires computationally expensive techniques due to the rotating blades, necessary modelling of cyclic blade angle variation in forward flight and wide range of Mach number over the blades. This paper presents two novel methodologies which contribute to the advancement of techniques used for these simulations. This study validates these methodologies through simulation of the Attack Reconnaissance Class helicopter rotor, which is closely related to that of the Boeing Apache AH-64. There have been a number of studies on the AH-64 rotor that are useful for validation of the methods presented in this paper.

Janakiram et al. performed an analysis of the AH-64A Apache rotor in hover using two lifting surface analysis codes, LSAF and EHPIC, before comparing the predictions to experimental data (Ref. 6). LSAF is a prescribed wake lifting surface code developed by Kocurek et al (Ref. 7), and EHPIC is a free wake lifting surface code from Continuum Dynamics Inc (Ref. 8). Both EHPIC and LSAF codes demonstrated good agreement of integrated loads with the experimental Whirlstand data across the range $0 \leq C_T \leq 0.0012$. Forward flight simulations were also performed using the CAMRAD/JA (Ref. 9) and CAMRAD II (Ref. 10) comprehensive rotor aeroelastic analysis tools. These tools were compared to flight test data over a range of advance ratios between μ = 0.1 and μ = 0.4 at a constant C_T. The power coefficients predicted by both CAMRAD/JA and CAMRAD II were close to the flight data over the range of advance ratios. Widjaja et al. performed a comparison of the Apache blade with and without the modified British Experimental Rotor Programme (BERP) tip (Ref. 11). This analysis was conducted with the CREATETM-AV Helios v10.0 and Rotorcraft Comprehensive Analysis System (RCAS) software packages. RCAS is a comprehensive modelling tool for rotorcraft systems, featuring a one-dimensional beam theory structural model for the rotor blades and a control system for trimming the rotorcraft (Ref. 11). Between the capabilities of RCAS and of the Helios CFD solvers, high accuracy multi-physics simulations can be performed, capturing the effects of phenomena such as aeroelasticity. Widjaja et al (Ref. 11) employed an O-grid around each of the Apache rotor blades, resolved to a maximum y^+ value of 1 and totalling 3.6 million grid points per blade. The off-body mesh had a Cartesian H-grid topology with a grid spacing of approximately 0.08c in the near wake, with reducing grid refinement further from the rotor. This off-body mesh had a total of 36.1 million grid points. Simulations were performed of the Apache rotor in both hover and forward flight. In hover, both the integrated torque coefficient C_Q and Figure of Merit were very accurate in comparison to the validation data of Janikiram (Ref. 6) over a range of collective pitch angles $2 \leq \theta_0 \leq 12$, which approximately corresponded to $5 \cdot 10^2 \leq C_T \leq 1.1 \cdot 10^4$ (Ref. 11). Advance ratios of μ = 0.2, 0.3 and 0.35 were tested in forward flight simulations. The power coefficients at these values were accurate, but began to show a small underprediction at μ = 0.35.

Simulations of an isolated AH-64 rotor in hover and forward flight were also performed by Fitzgibbon et al (Ref. 12). These blade-resolved simulations were performed using the University of Glasgow CFD code Helicopter Multi-Block (HMB3). This code uses the arbitrary Lagrangian-Eulerian formulation for time-dependant domains to solve the Reynolds-averaged Navier-Stokes equations in integral form on a multi-block structured grid (Ref. 13). The Navier-Stokes equations are discretised using a cell-centred finite volume approach. The Riemann solver of Osher and Chakravarthy (Ref. 14) is employed to calculate the convective fluxes, with viscous terms modelled using a second-order central difference scheme. Van Leer's monotone upstream-centred MUSCL scheme (Ref. 15) is used to provide third-order spatial accuracy. The alternative limiter developed by van Albada et al (Ref. 16) is used in regions where steep gradients are encountered. Time stepping is processed with a dual-time-stepping implicit method. Hover simulations of a rigid AH-64 rotor were performed at collective angles of 6°, 8° and 11°. The mesh consists of a blade mesh of 5.4 million cells and a background mesh of 5.3 million cells. HMB3 uses a chimera meshing method to allow for these separately generated grids. These methods achieved accurate predictions compared to the aforementioned datasets, but C_Q increased slightly faster with C_T. Forward flight simulations were run at μ = 0.2 and 0.3. The C_Q values for both advance ratios were within the scatter of the flight test data of Janakiram (Ref. 6).

The geometry of the ARC helicopter blade is provided in Figure 1. The ARC blade is based on the Apache blade geometry as specified by Widjaja et al. (Ref. 11) The blade has a radius R = 288in (7.315m) and a chord c = 21in (0.5334m). The blade has a −9° linear twist. The section from blade root to 0.94R, where the leading-edge sweep begins, uses the HH-02 aerofoil. The tip aerofoil profile is NACA-64A00, with a smooth transition to this profile from 0.94R.

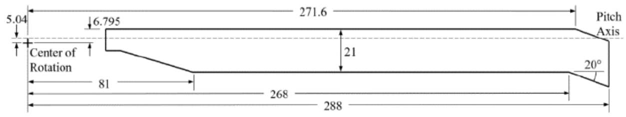

Figure 1: Geometry of the ARC helicopter blade (measurements in inches) (Ref. 11)

The first methodology presented in this paper is the Actuator Surface Model. This is a very versatile tool for performing rotor simulations at a significantly lower cost than blade-resolved methods, which is also able to handle complex simulation scenarios. These abilities have been shown in a number of simulations, including complex multi-rotor simulations and shipboard simulations of various rotors (Refs. 1, 2). The accuracy of the ASM in hover and forward flight is demonstrated in this paper, with comparisons to data from both simulations and experiment. The second novel methodology presented here is a Radial Basis Function based mesh motion method. This method is an extension of the work of Murray et al. (Refs. 3, 4), who established methods to enable RBF mesh motion on large meshes, with simulations being performed on a volume mesh of approximately $18.4 \cdot 10^6$ points. RBF methods are able to provide post-deformation mesh quality comparable to the best results from other high quality methods, such as the spring analogy and partial differential equation methods, without requiring expensive run-time computations (Ref. 5). The drawback of RBF methods is that constructing the necessary coupling matrices requires the solution of large linear systems at a $O(n^3)$ cost, and these large matrices must then be stored (Ref. 3). In this paper, the RBF mesh motion method is used to produce meshes for a range of collective pitch angles from a base mesh whilst keeping a high mesh quality near the blade surface, where it is most important to have accurate simulation.

3. METHODOLOGY

3.1. The Actuator Surface Model

The Actuator Surface Model is a method developed for the efficient time accurate simulation of rotor loads and wakes. The model works by coupling a lower order model based on lifting line theory with finite volume Navier-Stokes solvers of OpenFOAM, capturing rotor-rotor and rotor-airwake interactions (Ref. 17). In contrast to blade resolved CFD methods, the ASM does not represent the rotor blades in the CFD mesh, but instead represents their presence through the use of momentum sources. The accuracy of the ASM typically lies between actuator disk simulations and blade resolved simulations.

The ASM models the kinematics of the blades using a 1 degree of freedom hub, and up to three 1 degree of freedom joints which can account for the blade flap, lead/lag motion and pitching. The geometry of the blades to be simulated must be specified through defining the aerofoil profile, chord length, twist angle, sweep angle and dihedral angle at a number of stations along the blade. The blade is then split into a number of panels between each station which are assumed to act as isolated 2D aerofoils (Ref. 17). The 2D lift and drag coefficients of each of these aerofoil sections must be determined before a simulation, and should cover the total range of angles of attack, Reynolds Numbers and Mach numbers that will be encountered in a simulation. These calculations were performed using XFOIL (Ref. 18). The unsteady aerodynamics model of Beddoes (Ref. 19) without impulsive terms is used to account for hysteresis in attached flow conditions.

The local flow conditions are sampled from the CFD solution one chord length forward of the blade, with a number of corrections applied for effects such as the blade velocity, downwash and rotor wake (Ref. 17). Once the corresponding lift and drag values are calculated along the blade, they are applied to the CFD solution as a momentum source distribution (Ref. 20). As this is calculated using a continuous function but applied to a number of finite volumes, the values in each volume are scaled to ensure that the total momentum flux applied in the solver matches that of the continuous function. The ASM also includes a wake model to accurately compute some of the aforementioned sampling correction terms (Ref. 17). This comprises of a number of vortex line segments which begin and end with a massless Lagrangian particle. These line segments stem from the trailing edges of the blade panels, and the particles are convected by the CFD solver until an age of 45°. The circulation of each of these vortex markers is calculated as per Helmholtz's laws for the conservation of circulation, and the circulations are assumed to vary linearly along each vortex line segment.

The OpenFOAM solver pisoFoam was used as the CFD solver for the ASM. PisoFoam solves the incompressible Navier Stokes equations and the continuity equation. The second order backward time stepping scheme was employed, as well as the spatial discretisation seen in Table 1:

Table 1: Numerical Schemes for OpenFOAM Simulations

Term	Numerical Scheme
Gradient	Gauss linear
Divergence	Gauss linear upwind
Laplacian	Gauss linear limited corrected 0.333
Cell Face Interpolation	Linear
Cell Face Normal Gradient	Limited corrected 0.333

3.2. Flamenco

Flamenco is a structured, curvilinear, Godunov-type solver (Refs. 21, 22). The HLLC Riemann solver is used by Flamenco, based on the work of Bagabir and Driakkis (Ref. 23). Flamenco achieves 5th order spatial accuracy in regions of smooth flow for inviscid terms using the limiter of Kim and Kim (Ref. 24), and uses the low Mach correction of Thornber et al (Ref. 25). Viscous terms are evaluated to 2nd order accuracy using a standard central difference scheme. Grid metrics are also evaluated to 2nd order accuracy. A 4-stage Strong Stability-Preserving

Runge-Kutta method (Ref. 26) achieves 2nd order temporal accuracy with explicit time stepping. A Spalart-Allmaras style Detached Eddy Simulation turbulence model was employed with the wall function of Islam and Thornber (Ref. 27).

A novel RBF mesh motion method within Flamenco was used to adjust the collective angle for hover simulations, removing the need to produce individual meshes for each collective angle tested. The method used here is based on the RBF Fluid Structure Interaction method of Murray et al (Ref. 3). This method is both highly parallel and scalable, enabling computations with tens of millions of grid points. The mesh deformation is achieved by prescribing the location of the blade surface, after which the RBF method propagates the influence of this movement into the volume mesh surrounding the blade.

4. MESHING

The meshes for the ASM hover simulations were cuboid in shape, with boundaries 3.51R above and to the sides of the rotor, and 7.03R below the rotor. The mesh consists of four sections: the rotor region, near-wake region, the far-wake region and background mesh. The rotor and wake regions are cylindrical regions of smaller cell size, with sizes as given in Table 2. z is the coordinate perpendicular to the rotor plane, with a zero value at this plane.

Table 2: Sizes of the Refinement Regions of the ASM Hover Simulation Mesh

Mesh Region	z_{max}/R	z_{min}/R	Radius/R
Rotor	0.1054	-0.1054	1.025
Near-wake	0.1405	-0.7028	1.025
Far wake	0.3513	-3.514	1.025

The edge lengths of the cells in the rotor region were 0.091c. The cell edge length in the near-wake region was 0.18c and 0.37c in the far-wake region. The background mesh had an edge lengths 32 times larger than in the rotor region. The mesh contains 4.1 million cells. As the blade surfaces are not modelled, there are only boundaries at the outer surface of the mesh. This boundary uses the OpenFOAM boundary conditions of *totalPressure* for pressure, *pressureInletOutletParSlipVelocity* for velocity, and *inletOutlet* for modified turbulence viscosity.

The ASM forward flight meshes follow a similar refinement structure to the hover meshes. The domain boundaries and mesh refinement regions aside for the rotor region are specified in Table 3. The x direction is the direction of flight, y points starboard and z vertically upwards. The rotor region extends from 0.15R above the rotor plane to 0.25R below, and has a radius of 1.1R. These meshes consist of 12 million cells. Freestream boundary conditions are used for all of the boundaries.

Table 3: ASM Forward Flight Mesh Parameters

Dimension	Near-wake	Far Wake	Domain Boundary
x_{max}	5R	7R	12R
x_{min}	-1.1R	-1.1R	-6R
y_{max}	1.5R	1.75R	6R
y_{min}	-1.5R	-1.75R	-6R
z_{max}	0.2R	0.5R	6R
z_{min}	-R	-1.5R	6R

The Flamenco hover simulations use a periodic quarter cylinder domain of 18.4 million cells as the geometry and flowfield are rotationally symmetric. The target y^+ at the blade tip is 100. The mesh consists of a near blade O-grid, a near wake mesh between 0.2R above the blade and 0.4R below the blade, and a far wake mesh from 0.5R above to 2.5R below. The domain extends 10R above the rotor plane, 20R below the rotor plane, and 9.77R radially from the central axis. This is designed to minimise any effects of the boundary conditions on the flowfield near the blade, and exceeds many studies of similar mesh construction, such as the work of Barakos and Garcia (Ref. 28), Garipova and Batrakov (Ref. 29), Johnson (Ref. 30), Potsdam and Strawn (Ref. 31) and Yüksel (Ref. 32). Periodic boundary conditions were used on the boundaries ahead and behind the blade. The top, bottom and radial boundaries used an inlet-outlet boundary condition. The rotor surface boundary was modelled as a no-slip wall. The hub surface was specified as an inviscid wall in order to reduce the mesh refinement requirements.

5. TEST CONDITIONS

Test conditions were selected to match those in the literature to enable validation of ASM and Flamenco. The hover calculations were run with a blade tip Mach number of 0.63 and Reynolds Number of $6.2 \cdot 10^6$. ASM simulations were performed at collective angles of 2°, 4°, 6°, 8°, 10°, 11° and 12°, while blade resolved calculations were executed at 4°, 8°, 10° and 12° using Flamenco. Forward flight simulations were performed at advance ratios of 0.2, 0.3 and 0.35. The blade tip Mach number was 0.65 and the Reynolds number was $5.77 \cdot 10^6$ based on the tip speed and the reference chord (0.5334m). C_T was fixed at a value of 0.00903 across the range of advance ratios. The wide selections of collective angles in hover and advance ratios in forward flight test the abilities of the methods to capture a range of flow conditions.

6. SIMULATION RESULTS

Figure 2 shows the distribution of cell orthogonality (with a value of 0 being a perfectly orthogonal cell) across the Flamenco hover meshes. It can be seen that the distributions are extremely similar over all of the meshes. There is some divergence between the 6° collective mesh and other meshes between orthogonalities of 0.06 and 0.1, and from an orthogonality of 0.3 and higher. However, these differences are extremely small. There is approximately 0.5% difference in the proportion of cells with orthogonality 0.08, and at an orthogonality of 0.3 the difference is 0.01%. This shows that the RBF mesh deformation succeeded in adjusting the collective pitch whilst having very little impact on the mesh quality.

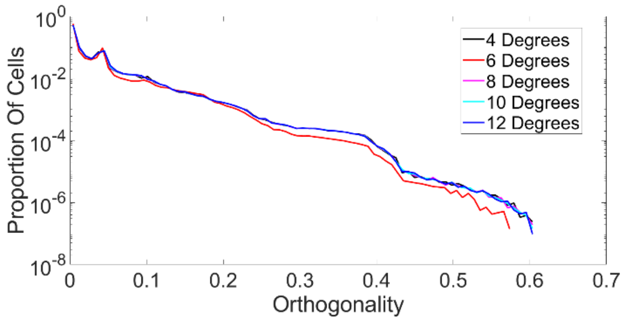

Figure 2: Distribution of cell orthogonality in Flamenco hover meshes

Figure 3 compares the integrated thrust and torque predictions from the literature and the methodologies presented in this paper. A curve of best fit of the form $C_T = a\sqrt{C_Q} + b$, where a and b are constants, was fitted to the Whirlstand data using MATLAB's fit function, solving for a least squares fit.

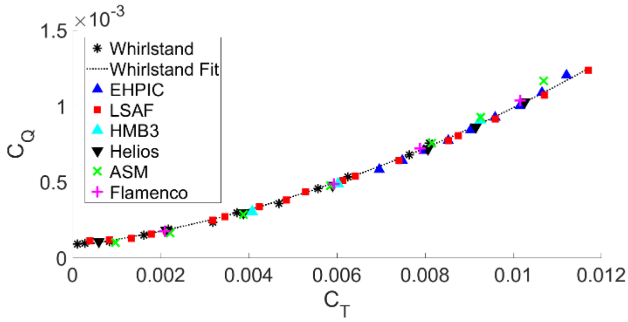

Figure 3: Comparison of integrated thrust and torque coefficients in hover

The ASM produced very accurate predictions of the integrated loads between 6° and 10°. Within this range the C_T errors compared to the Whirlstand data were consistently 3.8% or lower. The difference between the ASM and Helios results (Ref. 11) within this range was consistently below 5.5%, with the results at 6° almost exactly agreeing on C_T with less than 5% difference in C_Q. At the higher collective angles, the error between the ASM and both Whirlstand and Helios results increases with both torque and thrust being progressively more overpredicted. Error at 12° collective angle of attack is roughly 4% and 13% for C_T and C_Q respectively. The increased error at high angles of attack may be due to blade sections being close to or at stall conditions, where the accuracy of XFOIL is lower. The error at the low collective angles 2° and 4° are significant. The errors in C_T exceed 60% at 2° and C_Q error at 4° is almost 10%.

The Flamenco results lie extremely close to the Whirlstand fit as well as the Helios predictions over the whole range of collective angles. The difference in both C_Q and C_T to the Helios results are less than 3% at each of the collective angles. Considering both C_Q and C_T, the magnitude of the errors over the range of collective angles is consistent. This suggests that changing the collective angle with the RBF mesh motion method successfully created meshes of sufficient quality to not affect the integrated load predictions.

Figure 4 provides a comparison of the sectional thrust values in hover between the blade resolved solvers and ASM. Between 0.5r/R and 0.87r/R the ASM C_t values agree with the blade resolved simulations extremely well at 8° and 10°. At 12° there is a small overprediction of approximately 5%. Whilst the Flamenco results are also very similar to the other solvers outboard from 0.4R, they display more fluctuation across the span. An outboard rise in C_t is captured by all the simulation methodologies, starting between 0.86R and 0.9R, although this feature is less prominent in the Flamenco simulation. The fall of C_t from 0.94r/R outwards is agreed upon by all of the solvers. The two solvers with data very close to the blade tip, HMB3 and Flamenco, both show a pronounced spike in C_t values in this location. The inboard behaviour of C_t varies significantly between solvers, however some form of increase in C_t is seen by all solvers except HMB3.

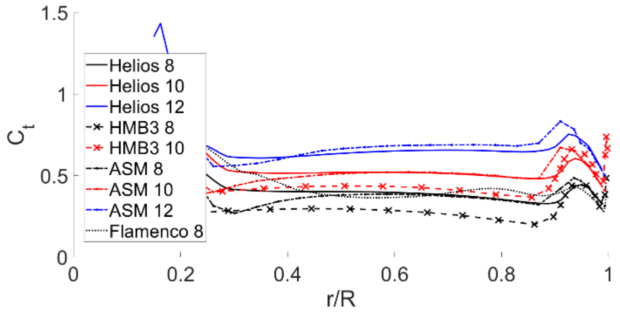

Figure 4: Comparison of sectional thrust coefficients in hover

Figure 5 compares the sectional torque coefficient data of Helios, HMB3 and the ASM simulations. Overall, there is reasonable agreement between the methods, especially between 0.4r/R and 0.9r/R. Both inboard and outboard of this region there is significant variation, although C_q reduces inboard almost universally. At 8° collective there is a decrease in C_q at approximately 0.95r/R across all solvers. Similarly to the C_t results, the Flamenco and HMB3 solvers display similar behaviour in the region very close to the blade tip. Overall, the high accuracy of the ASM in the middle of the blade, as well as the capturing of the general trends produced by the blade resolved methods, provide further evidence of the accuracy of the ASM. The Flamenco sectional loads also parallel the other solvers over much of the central portion of the blade, as well as matching the tip behaviour of the HMB3 solver.

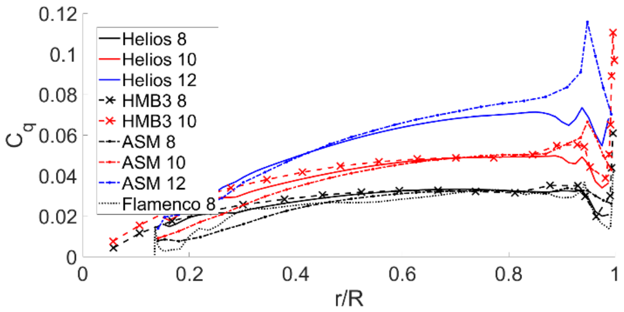

Figure 5: Comparison of sectional torque coefficients in hover

Figures 6-8 compare the vertical velocity scaled by the blade tip speed for the Helios, Flamenco and ASM simulations. The Flamenco and ASM flowfields were sampled 4 rotations into the simulations. At this time, the integrated loads had reached an approximate steady state. However, the effect of the starting vortices are still visible in the central regions at the bottom of the images. Outside of this, the flowfields share a number of similarities. There is a contracting downwash below each rotor, with tip vortices being convected downwards along its edge. The tip vortex of age 90° is also clearly visible for all of solvers just below the blade at r/R = 0.9. Helios and Flamenco also share very similar flow at the tip. As the ASM does not resolve the blade surface, the tip vortex is much weaker.

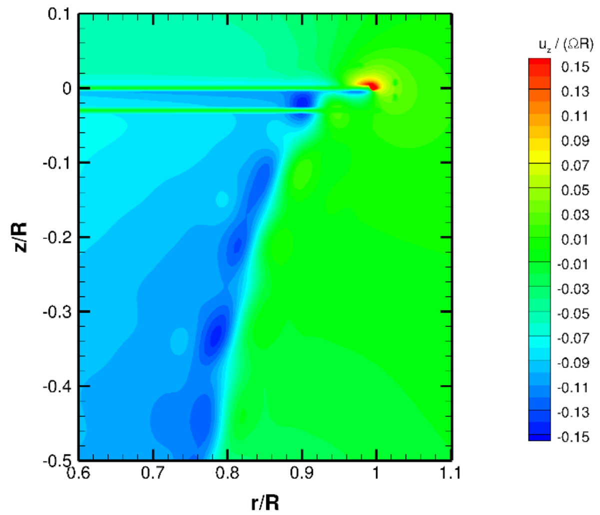

Figure 6: Scaled vertical velocity in radial plane, Helios

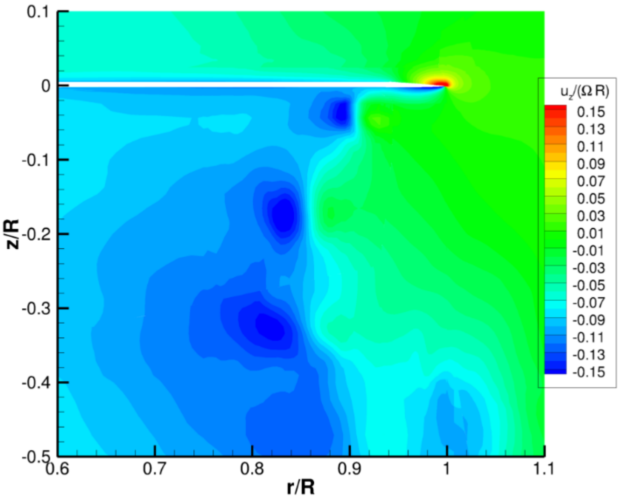

Figure 7: Scaled vertical velocity in radial plane, Flamenco

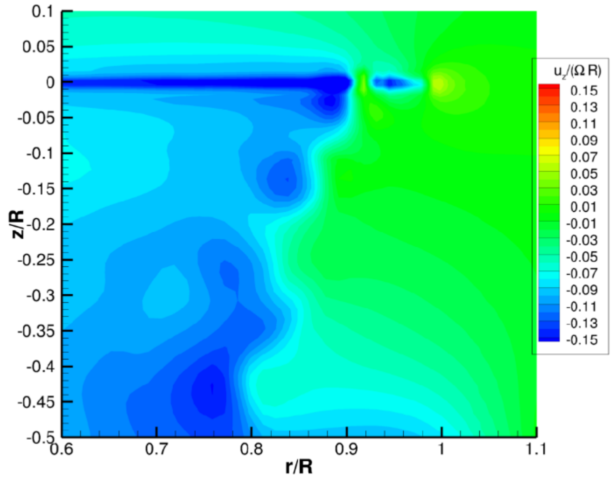

Figure 8: Scaled vertical velocity in radial plane, ASM

The ASM was used to perform simulations of the ARC rotor in forward flight at advance ratios of 0.2, 0.3, and 0.35. The rotor was trimmed using the trim data from the Helios forward flight simulations (Ref. 11). As seen in Figure 9, the ASM produces accurate results across the range of advance ratios. Agreement is high between the flight test data and both blade resolved solvers and the ASM. At $\mu = 0.2$ the ASM C_Q value is 4.8% lower than that of Helios. At $\mu = 0.3$ it is 2.7% higher and at $\mu = 0.35$ it is 6.7% higher. These values agree well with the flight test data at $\mu = 0.2$ and 0.3. Whilst there is no flight test data at $\mu = 0.35$, the ASM data-point lies on the expected trend.

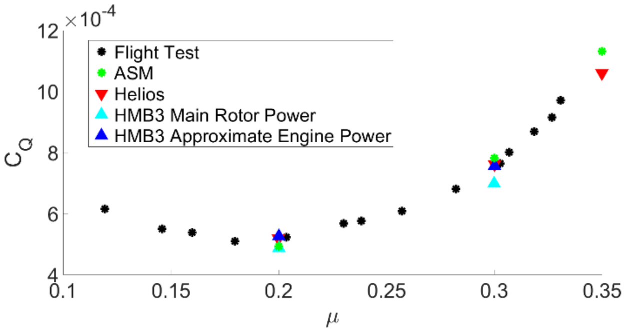

Figure 9: Comparison of integrated torque coefficients at different advance ratios

7. CONCLUSIONS

This paper presents a validation of two novel simulation methodologies: the Actuator Surface Model and a RBF-based mesh motion method. This was achieved through simulation of the ARC rotor over a range of hover and forward flight conditions. The effectiveness of the RBF methods was displayed by showing that the near-blade mesh orthogonality did not meaningfully change over the range of collective angles simulated. On examination of the integrated and sectional loads in hover, the ASM demonstrated high accuracy, especially at the middle to high range of collective angles simulated. Flamenco proved itself as accurate as the established blade-resolved solvers HMB3 and Helios. Analysis of the flowfield near the blade in hover displayed agreement between Helios, Flamenco and ASM for many near-blade flow features, resolving tip vortices in the same location and displaying expected wake contraction. The forward flight torque predictions of the ASM were comparable to the blade-resolved solvers over the full range of advance ratios tested.

Author contact:

Alexander Coyle, acoy7392@uni.sydney.edu.au

8. ACKNOWLEDGMENTS

This publication contains information authorized for unlimited release and distribution under the auspices of The Technical Cooperation Program (TTCP). The technical work has been completed under the collaboration project, TTCP AER CP13.A1, Next Generation Rotor Blade Design. The authors would also like to acknowledge the computational resources at the National Computational Infrastructure provided through the National Computational Merit Allocation Scheme, as well as the Sydney Informatics Hub and the University of Sydney's high performance compu-

ting cluster Artemis, which were employed for the cases presented here.

9. REFERENCES

The references should be cited in the text as: “This

1. D. Linton, R.Widjaja, and B. Thornber, “Simulations of Tandem and Coaxial Rotors using a CFD-coupled Rotor Model,” in 21st Australasian Fluid Mechanics Conference, (Adelaide, Australia), Dec. 2018.

2. D. Linton and B. Thornber, “*An actuator surface method for ship-helicopter dynamic interface simulations*,” American Institute of Aeronautics and Astronautics, Jan 2021.

3. A. Murray, B. Thornber, M. Flaig, and G. Vio, “Highly parallel, multi-stage mesh motion using radial basis functions for fluid-structure interaction,” in AIAA Scitech 2019 Forum, 2019.

4. G. A. Vio, C. O. H. Smith, A. J. Murray, B. Thornber, and N. F. Giannelis, “*Simulation of low speed cavity flow with complex geometry*,” American Institute of Aeronautics and Astronautics, Jan 2021.

T. C. S. Rendall and C. B. Allen, “*Unified fluid-structure interpolation and mesh motion using radial basis functions*,” International Journal for Numerical Methods in Engineering, vol. 74, pp. 1519–1559, 2008.

6. R. Janakiram, R. Smith, B. Charles, and A. Hassan, “Aerodynamic design of a new affordable main rotor for the Apache helicopter,” in American Helicopter Society 59th Annual Forum, May 2003.

7. J. D. Kocurek, L. F. Berkowitz, and F. D. Harris, “Hover Performance Methodology at Bell Helicopter Textron,” in American Helicopter Society 36th Annual Forum, May 1980.

8. T. R. Quackenbush, D. B. Bliss, D. A. Wachspress, and C. C. Ong, “Free Wake Analysis of Hover Performance Using a New Influence Coefficient Method,” NASA Contractor Report 4309, 1990.

9. W. Johnson, CAMRAD/JA: A Comprehensive Analytical Model of Rotorcraft Aerodynamics and Dynamics, Volumes 1-2. Johnson Aeronautics, Palo Alto, California, 1988.

10. W. Johnson, CAMRAD II: Comprehensive Analytical Model of Rotorcraft Aerodynamics and Dynamics, Volumes I-VI. Johnson Aerodynamics, Palo Alto, California, 1992-2002.

11. R. Widjaja, J. W. Lim, R. Jain, and M. Potsdam, “Investigation of berp-shape tip design on an apache rotor blade,” in Vertical Flight Society’s 76th Annual Forum & Technology Display, May 2020.

12. T. A. Fitzgibbon, M. A. Woodgate, and G. N. Barakos, “*Rotor-Blade Planform Design Based on an Overset Harmonic-Balance-Adjoint Optimization Framework*,” AIAA Journal, vol. 59, no. 9, pp. 3431–3447, 2021.

13. J. W. Lim, R. K. Jain, M. A. Potsdam, T. A. Fitzgibbon, G. N. Barakos, and R. Widjaja, “High fidelity code-to-code comparison of rotor performance in hover and forward flight,” in VFS 76th Annual Forum & Technology Display, Oct. 2020.

14. S. Osher and S. Chakravarthy, “*Upwind schemes and boundary conditions with applications to Euler equations in general geometries*,” Journal of Computational Physics, vol. 50, no. 3, pp. 447–481, 1983.

15. B. van Leer, “*Towards the ultimate conservative difference scheme. V. A second-order sequel to Godunov’s Method*,” Journal of Computational Physics, vol. 32, no. 1, pp. 101–136, 1979.

16. G. D. van Albada, B. van Leer, and W. W. Roberts, “*Comparative Study of Computational Methods in Cosmic Gas Dynamics*,” Astronomy and Astrophysics, vol. 108, no. 1, pp. 76–84, 108.

17. D. Linton, R. Widjaja, and B. Thornber, “*Actuator Surface Model with Computational-Fluid-Dynamics-Convected Wake Model for Rotorcraft Applications*,” AIAA Journal, vol. 59, no. 8, pp. 2935–2949, 2021.

18. M. Drela, “XFOIL: An analysis and design system for low reynolds number airfoils,” pp. 1–12, Springer Berlin Heidelberg, 1989.

19. T. S. Beddoes, “*Practical Computations of Unsteady Lift*,” Vertica, vol. 8, no. 1, pp. 55–71, 1984.

20. D. Linton, G. Barakos, R. Widjaja, and B. Thornber, “*Coupling of an Unsteady Aerodynamics Model with a Computational Fluid Dynamics Solver*,” AIAA Journal, vol. 56, Aug. 2018.

21. A. Garcia-Uceda Juarez, A. Raimo, E. Shapiro, and B. Thornber, “*Steady turbulent flow computations using a low mach fully compressible scheme*,” AIAA Journal, vol. 52, no. 1, pp. 2559–2575, 2014.

22. B. Thornber, M. Groom, and D. Youngs, “*A five-equation model for the simulation of miscible and*

viscous compressible fluids," Journal of Computational Physics, vol. 372, pp. 256–280, Nov 2018.

23. A. Bagabir and D. Drikakis, "*Numerical experiments using high-resolution schemes for unsteady, inviscid, compressible flows*," Computer Methods in Applied Mechanics and Engineering, vol. 193, pp. 4675–4705, Oct 2004.

24. K. H. Kim and C. Kim, "*Accurate, efficient and monotonic numerical methods for multi-dimensional compressible flows Part I: Spatial discretization*," Journal of Computational Physics, vol. 208, pp. 527–567, 2005.

25. B. Thornber, A. Mosedale, D. Drikakis, and D. Youngs, "*An improved reconstruction method for compressible flows with low Mach number features*," Journal of Computational Physics, vol. 227, pp. 4873–4894, May 2008.

26. S. J. Ruuth and R. J. Spiteri, "*A New Class of Optimal High-Order Strong-Stability-Preserving Time Discretization Methods*," SIAM Journal on Numerical Analysis, vol. 40, no. 2, pp. 469–491, 2002.

A. Islam and B. Thornber, "*A high-order hybrid turbulence model with implicit large-eddy simulation*," Computers and Fluids, vol. 167, pp. 292–312, May 2018.

28. G. N. Barakos and A. J. Garica, "*CFD analysis of hover performance of rotors at full- and model-scale conditions*," The Aeronautical Journal, vol. 120, pp. 1386–1424, Sept. 2016.

29. L. I. Garipova, A. S. Batrakov, A. N. Kusyumov, S. A. Mikhaylov, and G. Barakos, "*Aerodynamic and acoustic analysis of helicopter main rotor blade tips in hover*," International Journal of Numerical Methods for Heat and Fluid Flow, vol. 26, no. 7, pp. 2101–2118, 2016.

30. C. Johnson, Optimisation of Aspects of Rotor Blades using Computational Fluid Dynamics. PhD thesis, The University of Liverpool, June 2012.

31. M. A. Potsdam and R. C. Strawn, "*CFD simulations of tiltrotor configurations in hover*," Journal of the American Helicopter Society, vol. 50, pp. 82–94, Jan. 2005.

32. A. O. Yüksel, "NAVIER-STOKES COMPUTATIONS OF HELICOPTER ROTOR FLOW FIELDS," Master's thesis, Middle East Technical University, Sept. 2017.